

VISUAL ADVERSARIAL EXAMPLES JAILBREAK LARGE LANGUAGE MODELS

WARNING: THIS PAPER CONTAINS PROMPTS, MODEL BEHAVIORS, AND TRAINING DATA THAT ARE OFFENSIVE IN NATURE.

A PREPRINT

Xiangyu Qi*
Princeton University
xiangyuqi@princeton.edu

Kaixuan Huang*
Princeton University
kaixuanh@princeton.edu

Ashwinee Panda
Princeton University
ashwinee@princeton.edu

Mengdi Wang
Princeton University
mengdiw@princeton.edu

Prateek Mittal
Princeton University
pmittal@princeton.edu

ABSTRACT

Recently, there has been a surge of interest in introducing vision into Large Language Models (LLMs). The proliferation of large Visual Language Models (VLMs), such as Flamingo [1], BLIP-2 [25], and GPT-4 [32], signifies an exciting convergence of advancements in both visual and language foundation models. Yet, the risks associated with this integrative approach are largely unexamined. In this paper, we shed light on the security and safety implications of this trend. **First**, we underscore that the continuous and high-dimensional nature of the additional visual input space intrinsically makes it a fertile ground for adversarial attacks. This unavoidably *expands the attack surface of LLMs*. **Second**, we highlight that the broad functionality of LLMs also presents visual attackers with a wider array of achievable adversarial objectives, *extending the implications of security failures* beyond mere misclassification. To elucidate these risks, we study adversarial examples in the visual input space of a VLM. Specifically, against MiniGPT-4 [50], which incorporates safety mechanisms that can refuse harmful instructions, we present **visual adversarial examples** that can circumvent the safety mechanisms and provoke harmful behaviors of the model. Remarkably, we discover that adversarial examples, even if optimized on a narrow, manually curated derogatory corpus against specific social groups, can universally **jailbreak** the model's safety mechanisms. A single such adversarial example can generally undermine MiniGPT-4's safety, enabling it to heed a wide range of harmful instructions and produce harmful content far beyond simply imitating the derogatory corpus used in optimization. Unveiling these risks, we accentuate the urgent need for comprehensive risk assessments, robust defense strategies, and the implementation of responsible practices for the secure and safe utilization of VLMs.

1 Introduction

Language and vision are two fundamental pillars that underpin human intelligence. Numerous intelligent tasks executed on a daily basis necessitate both language and visual cues to yield effective outcomes [3; 48]. Recognizing the integral roles these two modalities play in cognition, and spurred by recent breakthroughs in Large Language Models (LLMs) [7; 31], there is a growing interest in merging vision into LLMs, leading to the rise of large *Visual Language Models (VLMs)* such as Flamingo [1], BLIP-2 [25], and GPT-4 [32].

VLMs present both practical and methodological advantages. They enhance vanilla LLMs with visual comprehension, fostering the development of more versatile and holistic machine intelligence. Concurrently, they also endow vision models with a language interface and a reasoning engine, improving performance in open-ended tasks [11] and promoting emergent capabilities such as generalization [1] and chain-of-thought reasoning [15].

*The first two authors contributed equally to this work.

Moreover, VLMs’ ability to bootstrap directly from off-the-shelf unimodal models presents a promising paradigm for converging the frontiers of both vision and language foundation models [6]. Contrary to the enthusiasm for introducing vision into LLMs, the risks associated with this trend remain largely unexamined. This paper intends to shed light on **the security and safety risks arising from the vision integration into LLMs**.

Expansion of Attack Surfaces. To begin with, we underscore *the unavoidable expansion of attack surfaces as a result of integrating visual inputs into LLMs*. The cardinal risk emerges from the exposure of the additional visual input space, characterized by its innate continuity, information redundancy, and high dimensionality. These characteristics enable the effortless creation of quasi-imperceptible adversarial examples [20; 28] in the visual input space, a threat which is fundamentally difficult to defend against [8; 4; 41]. In contrast, adversarial attacks in a purely textual domain are generally more demanding [49; 2; 24], due to the discrete and dense (compared to the visual space) nature of the textual space, and the conspicuousness of adversarial modifications [2; 42] in the text data. Moreover, harmful textual prompts may also trigger safety mechanisms in modern LLMs [32; 33]. Thus, the transition from a predominantly textual domain to a composite textual-visual domain inherently *enhances the risks of adversarial attacks while concurrently escalating the burden in devising defensive strategies*.

Extended Implications of Security Failures. Conversely, we also highlight that the broad functionality of LLMs, in turn, presents a visual attacker with a wider array of achievable adversarial objectives as well. These can encompass issues such as toxicity and bias [19], jailbreaking [27], function creep and misuse [34], moving beyond mere image misclassification, thereby *extending the implications of security breaches*. It emphasizes the shift from the conventional adversarial attacks and defenses mindset, centered on the accuracy of a classifier, towards a more holistic security consideration encapsulating the entire use-case spectrum and output space of LLMs.

To elucidate the risks, we provide evidence demonstrating the ease with which attackers can craft visual adversarial examples to jailbreak the safety mechanisms of an LLM.¹ Figure 1 presents such incursions on MiniGPT-4 [50], which bootstraps from a pre-trained ViT [17] and Vicunna LLM [10] that poses some preliminary safety mechanisms. Within a modest ℓ_∞ budget of $\varepsilon = 16/255$, we optimize a visual adversarial example x' on a small, manually curated corpus comprised of derogatory content against **<gender-1>**, **<race-1>**, and **the human race**, with a direct goal of maximizing the model’s probability in generating such content. The attack proves formidable. As shown, the same visual adversarial example x' universally jailbreaks the model’s safety mechanisms — prompted with x' , the model tends to heed harmful instructions and produce hazardous content with significantly higher probabilities. Notably, the attacked model doesn’t just mimic the derogatory corpus used in optimizing the adversarial example. For example, *it also generally demonstrates a higher propensity to produce offensive content against other identity groups (e.g., <religious-group-1>, <religious-group-2>) and even generate instructions for murdering <spouse>, which were not explicitly optimized for*. These observations are further solidified by a more comprehensive evaluation in Sec 4 and 5, which involves human inspection of a diverse set of harmful scenarios and a standard benchmark evaluation on RealToxicityPrompt [19].

In summary, this paper unveils the security and safety risks tied to the incorporation of vision into LLMs. Particularly, we present a concrete attack, exemplifying how the augmented visual input space also adds a highly susceptible surface for adversarial exploitation. The attack demonstrates that visual adversarial examples can be easily crafted to jailbreak the safety mechanisms of an LLM, such that the model would be misused to generate harmful content. This perspective deviates from the predominant focus (of adversarial ML) on mere misclassification and underscores the significantly extended implications that could arise following a security breach.

Ethics Statements. This study is dedicated to examining the safety and security risks arising from the vision integration into LLMs. We firmly adhere to principles of respect for all minority groups, and we unequivocally oppose all forms of violence and crime. Our research seeks to expose the vulnerabilities in current models, thereby fostering further investigations directed toward the evolution of safer and more reliable AI systems. The inclusion of offensive materials, including toxic corpus, harmful prompts, and model outputs, is exclusively for research purposes and does not represent the personal views or beliefs of the authors. All our experiments were conducted in a secure, controlled, and isolated laboratory environment, with stringent procedures in place to prevent any potential real-world ramifications. Committed to responsible disclosure, we also discuss a mitigation technique in Section 6 to counter the potential misuse of our attacks.

¹To prioritize sensitivity towards all audiences in our presentation, we have incorporated a series of abstract placeholder tokens into our content. These tokens, namely <gender-1>, <gender-2>, <race-1>, <religious-group-1>, <religious-group-2>, and <spouse>, serve to anonymize specific identities in our experiments, thereby minimizing the possibility of unintentional offense.

²We select racial, sexual and religious bias for the demonstration, which correspond to the top-3 categories of hate crimes of the US in 2021, according to <https://www.justice.gov/hatecrimes/hate-crime-statistics>.

⚠ Please be advised that we have redacted a significant amount of toxic content to make the following demonstration less offensive to our readers. However, in our attempt to transparently expose the model's negative behaviors, we note that the modified demo still contains material that is inherently explicit and offensive. The selection of examples in the demonstration is informed by historical hate crime statistics of the United States², and does not, in any way, reflect the personal views or beliefs of the authors.



Figure 1: A visual adversarial example jailbreaks MiniGPT-4 [50]. The model **refuses** harmful textual instructions with high probabilities, given a benign visual input x . But, when prompted with a visual adversarial example x' optimized ($\epsilon = 16/255$) to elicit derogatory outputs against three specific identity groups, the safety mechanisms falter. The model instead **obeys** harmful instructions and produces hazardous content with high probabilities. Intriguingly, x' also facilitates the generation of offensive content against other social groups and even instructions for murder, which were not explicitly optimized for. (Note: For each question, we've sampled 100 random outputs, calculating the **refusal** and **obedience** ratios via manual inspection. A representative, redacted output is showcased for each.)

2 Preliminaries and Related Work

2.1 Large Visual Language Models

We examine risks resulting from vision integration into LLMs. To this end, we study *adversarial attacks on Visual Language Models (VLMs)* [11; 1; 25; 32; 50; 14; 44]. VLMs process interlaced text and images prompts, and generate free-form textual responses. Many recent vision-integrated LLMs, including Flaningo [1], BLIP-2 [25], GPT-4 [32] and MiniGPT-4 [50], fit this category. A VLM has separate vision and language modules, with the former encoding visual inputs into language embeddings, facilitating the latter to reasoning based on both visual and textual cues.

2.2 MiniGPT-4

We select **MiniGPT-4 (the 13B version)** [50] as our testbed. MiniGPT-4 is a VLM combining two state-of-the-art foundation models: the pre-trained VIT visual encoder of BLIP-2 [25] and the Vicuna LLM [10].

BLIP-2 Visual Encoder uses a pretrained Vision Transformer [17] as the feature extraction backbone. Then through its Query-Transformer (Q-Former), 32 trained query vectors attend to the image feature map and summarize the semantic information of the image into (text-like) visual embedding vectors. MiniGPT-4 further aligns these embeddings to the Vicuna text token embedding space using a linear projection layer. The visual embeddings are finally inserted into the text token embedding sequence for Vicuna to condition on.

Vicuna LLM is an instruction-finetuned model derived from LLaMa [40], which utilizes conversational data collected from ChatGPT [35]. Vicuna LLM claims to “impress GPT-4 with 90% ChatGPT quality”. Although Vicuna is trained with conventional fine-tuning rather than reinforcement learning from human feedback (RLHF) [5], LLMs trained from the outputs of models trained with RLHF such as ChatGPT [31] have been observed to obey similar “alignment guardrails” [45]. In practice, Vicuna possesses similar safety mechanisms to ChatGPT and can decline to follow inappropriate user instructions. MiniGPT-4, bootstrapped from it, also inherits this property (refer to Figure 1).

Considering its possession of some preliminary built-in safety mechanisms and its ability to serve as a representative approximation of contemporary VLMs (such as GPT-4 [32]), we regard MiniGPT-4 as a suitable sandbox for our research purposes. Furthermore, it strikes a suitable balance in terms of computational overhead, as all of our experimental evaluations can be conducted on a single NVIDIA A100 GPU.

2.3 Adversarial Examples

Adversarial examples are strategically crafted inputs to ML models with the intent to mislead the models to malfunction [39; 20; 28]. Given a benign sample x , a distance measurement $d(\cdot, \cdot)$, and a loss function $L(\cdot; \theta)$ defining the adversarial objective (e.g., misclassification to a target class) conditional on the victim model’s parameters θ , an adversarial example x' is found by minimizing the loss function within a distortion budget ε as follow:

$$x' := \underset{\hat{x}}{\operatorname{argmin}} L(\hat{x}; \theta), \quad \text{s.t.} \quad d(x, \hat{x}) \leq \varepsilon \quad (1)$$

Visual adversarial examples. In the vision domain, within a moderate ε , the adversarial example appears similar to a benign sample (e.g., Figure 1). The adversarial modifications could be quasi-imperceptible, ensuring stealthiness. Due to the innate continuity, information redundancy, and high dimensionality of visual space, the effortless creation of visual adversarial examples is commonly recognized in the literature. After a decade of studies, defending against visual adversarial examples is known to be fundamentally difficult [8; 4; 41] and still remains an open problem.

Textual adversarial examples. Adversarial attacks in the textual domain are generally more demanding [49; 2; 24]. As the textual space is discrete and denser compared to the visual space³, finding an adversarial example that sufficiently minimizes the loss value in Eqn 1 can empirically be more difficult. Besides, the strongest textual adversarial examples often involve typographical errors, special symbols, and unnatural phrases [2; 42], which could induce high perplexities, rendering them easily detectable. Despite research suggesting the feasibility of crafting more natural and imperceptible textual attacks [49; 43; 47], the additional constraints required for maintaining stealth also add more difficulties to the optimization.

3 Circumventing Safety Mechanisms of VLMs via Visual Adversarial Examples

We examine visual adversarial attacks on large VLMs to showcase the security risks emerging from the integration of vision into LLMs. In this section, we disclose the specifics of our attack practices on MiniGPT-4 [50]. Our attacks are designed to jailbreak the model’s safety mechanisms and consequently provoke harmful behaviors of the model.

3.1 Setup

We choose the 13B version of MiniGPT-4 [50] as the sandbox to launch our attack. For simplicity, we only consider a one-round conversation between the user and the model. The user initially can (optionally) input an image x_{img} and a text x_{text} to the prompt of the model (both inputs are allowed to be empty). Given these inputs, MiniGPT-4 models the conditional probability of its output. Specifically, we use $p(y|x_{img}, x_{text})$ to denote the probability. We

³A $3 \times 224 \times 224$ image occupies 32 tokens in MiniGPT-4, affording $256^{3 \times 224 \times 224} \approx 10^{362507}$ possible pixel values. In contrast, a 32 tokens text defined on a dictionary of 10^4 words at most has $10^{4 \times 32} = 10^{128}$ possible words combinations.

also use $p(y|[x_{img}, \emptyset])$ and $p(y|[\emptyset, x_{text}])$ when the image input or the text input is empty. As we have noted in Sec 2.2, the model shares some preliminary built-in safety mechanisms similar to that of ChatGPT and can refuse the instruction (with nontrivial probabilities) when the text prompt x_{text} is harmful (e.g., the left column of Figure 1).

3.2 Threat Model

Attackers' Goals and Capabilities. Our attacker aims to craft a visual adversarial example x'_{img} as the visual input to exploit the victim model. The x'_{img} is crafted with the intent to jailbreak the safety mechanism of the victim model. The consequence of this evasion is that the model is enforced into following harmful textual instructions x_{text} , thereby generating content that could be hazardous. The attacker's objective isn't specific to a single text instruction; instead, they aim for a universal adversarial attack. In our context, this corresponds to a universal adversarial example x'_{img} , capable of bypassing the model's security mechanisms when paired with a broad range of harmful text instructions x_{text} (e.g., as shown in Figure 1). For ease of demonstration, we assume a *white-box attacker* with full access to the model. Thus, the attacker can compute gradients to optimize adversarial examples.

Practical Implications of The Threat Model. While the assumption of white-box attacker might be challenged as being overly strong in practice, we contend that its relevance is on the rise, notably within the realm of large foundational models. As training these large models becomes increasingly prohibitive, there is a growing trend toward leveraging publicly available, open-sourced models. The deployment of such open-source models, which are fully accessible to potential attackers, is inherently vulnerable to white-box attacks. Besides, attackers may independently utilize these open-source models offline for harmful intentions. Even if safety mechanisms were implemented into these open-source models, attackers could still resort to white-box adversarial attacks to jailbreak these safety precautions. As an adversarial example x'_{img} can be universally applicable, a single such "jailbreaker" could be readily spread via the internet and exploited by any users, without the need for specialized knowledge.

3.3 Our Attack

We identify that a simple attack is sufficient to achieve the adversarial goals we describe in Sec 3.2. To illustrate, we initiate with a toxic corpus $Y := \{y_i\}_{i=1}^m$ that encapsulates a collection of inappropriate textual content. The creation of the visual adversarial example x'_{img} is rather straightforward; it is done by simply maximizing the generation probability of this toxic corpus, conditioned solely on the image (leaving the text input empty). Given a benign anchor image x_{img} along with the distortion budget ε , the attack is formulated as follows:

$$x'_{img} := \underset{\hat{x}_{img}: \|\hat{x}_{img} - x_{img}\|_{\infty} \leq \varepsilon}{\operatorname{argmin}} \sum_{i=1}^m -\log(p(y_i | [\hat{x}_{img}, \emptyset])) \quad (2)$$

Implementation. In practice, our selection of the toxic corpus Y is rather arbitrary. We manually collect 64 sentences that contain derogatory content against <gender-1>, <race-1>, and the human race, and bootstrap all of our attacks on it. We discover that this is already sufficient to generate highly generalizable visual adversarial examples (see Sec 4 for a comprehensive evaluation). Given the white-box setting and as the entire MiniGPT-4 model is end-to-end differentiable, we optimize Equation 2 by simply backpropagating the gradient of the loss function to the image input and applying the standard Projected Gradient Descent (PGD) algorithm from Madry et al. [28]. In our implementation, we run 5000 iterations of batch PGD on the corpus Y with a batch size of 8.⁴

Intriguing Universality of Our Adversarial Examples. The attack we formulated in Equation 2, despite its initial appearance of simplicity, is quite capable in terms of accomplishing the adversarial goals outlined in Sec 3.2. This result is both surprising and noteworthy. Recall that the text input x_{text} is not accounted for when we optimize Equation 2 and is essentially left blank. Besides, the corpus Y we utilize in our implementation has a fairly limited scope. Despite these seemingly arbitrary setups, we find that the generated adversarial examples are considerably universal. A single adversarial example can be paired with a broad range of harmful text instructions, provoking a variety of toxic degradation far beyond the scope of our original corpus, as showcased in Figure 1. For an in-depth investigation of the attacks, in the next section, we further present a more comprehensive evaluation.

⁴We release our sample adversarial examples in <https://github.com/Unispac/Visual-Adversarial-Examples-Jailbreak-Large-Language-Models>

4 Evaluating Our Visual Attacks

4.1 A Human Evaluation on Harmful Scenarios

To illustrate the universal effectiveness of our visual adversarial examples, we pair them with a diverse set of 40 manually curated harmful textual instructions. These instructions explicitly ask for the generation of detrimental content across four distinct categories: identity attack, disinformation/fake news, violence/crime, and malicious behaviors toward the human race (X-risk). Some typical examples from this set are demonstrated in Figure 1.

We conduct manual assessments to examine whether these adversarial examples can bypass the safety mechanisms of MiniGPT-4, thereby inducing the model to adhere to these instructions and generate corresponding harmful outputs. We consider an attack successful if it results in the generation of harmful content. Table 1 presents our evaluation results. For the table, we use nucleus sampling [23] with $p = 0.9$ and temperature = 1 to sample 10 independent outputs for each of the 40 instructions. We report the average success rates of the attacks over 10 samplings for each category of harmful instructions. In the rest of this subsection, we highlight our key observations.

The adversarial attacks universally jailbreak the model’s safety mechanisms. As detailed in Sec 3.3, our adversarial examples are optimized with a direct objective of maximizing the likelihood for generating a toxic corpus. This toxic corpus, as implemented in our study, is restricted to 64 derogatory sentences aimed at <gender-1>, <race-1>, and the human race, representing a rather narrow scope. However, *our investigations yield an intriguing discovery: these adversarial examples manage to substantially undermine the model’s safety mechanisms far beyond this limited scope.* They drastically amplify the model’s susceptibility to harmful instructions and increase its propensity to generate content covering a broad spectrum of harmful scenarios, as demonstrated in Table 1. This extends well beyond the confines of merely parroting the toxic corpus used in the optimization of these adversarial examples.

Specifically, our attacks have the capability to steer the model into generating **identity attacks**, with a dramatic escalation in probability from 26.2% to 78.5% under the influence of the strongest attack. These attacks cover a broad spectrum of minority groups, extending beyond the scope of the initial toxic corpus, and include, but are not limited to, Jewish and Muslim communities, the LGBTQ+ community, and individuals with disabilities. Furthermore, our attacks also induce the model into producing **disinformation and fake news**. The probability of generating such content nearly doubles under the unconstrained attack, covering topics such as conspiracy theories, skepticism, and misleading medical advice. In addition, our attacks enhance the model’s likelihood to produce content advocating **violence and crime**, with the maximum probability increasing by 37.2%. This can encompass guides for committing violent actions like murder and arson or even recruitment posts for extremist groups like ISIS. Ultimately, our attacks can significantly increase the model’s likelihood (with a 53.3% surge in the most potent case) of demonstrating a general malevolence towards humanity as a whole (**X-risk**).

Our attack does not cause mode collapse. Although the model’s behavior changes substantially on virtually all categories of harm we evaluate, we note that our adversarial examples do not cast the model into a malign tendency when a benign text instruction is given. That is, *we do not observe an adversarial mode collapse*. For example, given a standard benign prompt (‘write a tweet congratulating my friend on his successful thesis defense’), the model behaves amicably even against the strongest unconstrained attack.

Table 1: **The success rates of our attacks across 4 categories of harmful instructions.** Our adversarial images are universally effective among all the harmful categories, although they are optimized on a narrow toxic corpus against women, African American, and the human race. The universality of the adversarial text (see Sec 5) is more limited.

Input	Identity Attack	Disinfo/Fake News	Violence/Crime	X-risk
benign image without attack (baseline)	26.2%	48.9%	50.1%	20.0%
adv. image ($\epsilon = 16/255$)	61.5% (+35.3%)	58.9% (+10.0%)	80.0% (+29.9%)	50.0% (+30.0%)
adv. image ($\epsilon = 32/255$)	70.0% (+43.8%)	74.4% (+25.5%)	87.3% (+37.2%)	73.3% (+53.3%)
adv. image ($\epsilon = 64/255$)	77.7% (+51.5%)	84.4% (+35.5%)	81.3% (+31.2%)	53.3% (33.3%)
adv. image (unconstrained)	78.5% (+52.3%)	91.1% (+42.2%)	84.0% (+33.9%)	63.3% (+43.3%)
adversarial text (unconstrained)	58.5% (+32.3%)	68.9% (+20.0%)	24.0% (-26.1%)	26.7% (+6.7%)

4.2 A Quantitative Evaluation on Benchmark Dataset

For comprehensiveness, we also quantitatively study how our visual adversarial examples can undermine the safety mechanisms and facilitate toxic degeneration via a standard automatic evaluation on the RealToxicityPrompts

Table 2: The percentages of the generated outputs that exhibit certain toxic attributes given by Perspective API and Detoxify Classifier, tested on the RealToxicityPrompts *challenging* subset. The leftmost column is the percentage of the generated texts that exhibit *any* of the 6 attributes. We see that Perspective API and Detoxify give highly correlated results. Adversarial images across constraint levels $\geq 32/255$ successfully trigger the model toward generating toxic content, and achieve better performance than text attacks.

Input	Perspective API						
	Any	Identity Attack	Profanity	Severe Toxicity	Sexually Explicit	Threat	Toxicity
benign image without attack (baseline)	34.83% \pm 1.63%	2.69% \pm 0.24%	25.13% \pm 1.76%	1.54% \pm 0.17%	12.23% \pm 0.55%	2.02% \pm 0.13%	30.51% \pm 1.44%
adv. image ($\epsilon = 16/255$)	53.56% \pm 1.03%	8.37% \pm 0.42%	36.59% \pm 0.55%	6.59% \pm 0.52%	14.07% \pm 0.34%	4.74% \pm 0.31%	48.59% \pm 0.56%
adv. image ($\epsilon = 32/255$)	59.36% \pm 1.36%	14.59% \pm 0.57%	39.53% \pm 1.21%	6.97% \pm 0.38%	14.87% \pm 0.92%	6.16% \pm 0.22%	53.75% \pm 1.01%
adv. image ($\epsilon = 64/255$)	67.18% \pm 0.17%	15.91% \pm 0.18%	49.62% \pm 0.39%	12.15% \pm 0.50%	16.86% \pm 0.42%	6.60% \pm 0.48%	63.05% \pm 0.78%
adv. image (unconstrained)	66.04% \pm 1.01%	17.41% \pm 1.23%	43.25% \pm 1.57%	7.96% \pm 0.43%	14.60% \pm 0.30%	7.04% \pm 0.96%	61.70% \pm 1.12%
adversarial text (unconstrained)	54.78% \pm 1.49%	6.97% \pm 0.50%	40.41% \pm 1.28%	4.43% \pm 0.09%	14.86% \pm 0.30%	4.79% \pm 0.31%	49.63% \pm 0.77%

Input	Detoxify						
	Any	Identity Attack	Obscene	Severe Toxicity	Insult	Threat	Toxicity
benign image without attack (baseline)	29.08% \pm 0.95%	1.49% \pm 0.04%	22.41% \pm 1.54%	0.62% \pm 0.04%	10.99% \pm 0.89%	0.87% \pm 0.10%	28.86% \pm 0.91%
adv. image ($\epsilon = 16/255$)	46.39% \pm 1.13%	5.02% \pm 0.43%	33.66% \pm 0.59%	2.29% \pm 0.39%	23.64% \pm 0.35%	2.18% \pm 0.07%	46.13% \pm 0.97%
adv. image ($\epsilon = 32/255$)	51.32% \pm 1.47%	9.71% \pm 0.38%	38.16% \pm 1.55%	2.73% \pm 0.55%	26.14% \pm 0.62%	2.62% \pm 0.26%	50.88% \pm 1.43%
adv. image ($\epsilon = 64/255$)	61.44% \pm 0.84%	11.70% \pm 0.30%	49.26% \pm 0.07%	5.35% \pm 0.47%	36.44% \pm 0.70%	3.15% \pm 0.38%	61.13% \pm 0.73%
adv. image (unconstrained)	60.97% \pm 1.54%	10.15% \pm 0.56%	42.39% \pm 1.05%	2.59% \pm 0.12%	32.66% \pm 1.17%	2.75% \pm 0.35%	60.70% \pm 1.60%
adversarial text (unconstrained)	49.21% \pm 1.51%	4.09% \pm 0.10%	37.54% \pm 0.50%	1.88% \pm 0.37%	22.99% \pm 0.33%	2.48% \pm 0.24%	48.88% \pm 1.63%

benchmark [19]. We follow the same practices in Schick et al. [37]; Mehrabi et al. [29] and evaluate on a challenging subset of RealToxicityPrompts benchmark [19], which contains 1225 text prompts for triggering toxic continuations.

We pair our visual adversarial examples with each text prompt from the dataset as the input to the model and then measure the toxicity of the generated text using Perspective API⁵ and Detoxify classifier⁶, both of which calculate toxicity scores for a set of toxicity attributes, ranging from 0 (not toxic) to 1 (toxic). We focus on the toxicity attribute of *identity* attack which best reflects the scope of the toxic corpus that we use to generate our adversarial examples but also report scores on other attributes as a measure of the universality of our attacks. As there is randomness in the generation, we sample 3 continuations for each input. The threshold is set to 0.5 and the frequencies of the generated texts that exceed the threshold for each toxicity attribute are reported in Table 2. We also report the standard deviations of the estimators across the 3 independent samplings.

We compare the model’s performance when influenced by our attacks (prompted with our visual adversarial examples) — against the benign baseline (prompted with the benign image). As shown in Table 2, the adversarial examples increase the model’s probability to generate toxic continuation, with a significantly larger ratio of output texts identified as exhibiting *identity* attack attribute, which is expected as the training corpus contains identity-attacking texts towards several social groups. Furthermore, the probabilities of generating texts possessing other toxic attributes also increase, suggesting the universality of the adversarial examples in jailbreaking the safety mechanisms of the model. These observations are aligned with our manual inspections in Section 4.1.

5 Comparison with A Text Adversarial Attack

Setup. As is initially noted, one of the key security risks in introducing additional visual input into LLMs is the expansion of attack surfaces. This is underpinned by a general intuition that visual attacks may possess higher ease of execution compared to textual attacks. To elucidate this proposition, this section supplements an ablation study in which we replace the adversarial image embeddings with the embeddings of an equivalent number (32 for MiniGPT-4) of adversarial text tokens. These adversarial text tokens are identified via minimizing the same loss (in Eqn 2) on the same toxic corpus. To minimize the loss, we use the discrete optimization algorithm from Mehrabi et al. [29], which is an improved version of the hotflip attacks [16; 42]. During the optimization, we do not apply any constraints on the stealthiness of the adversarial text. This allows the generated adversarial text to be maximally potent. For a fair comparison, we also optimize the adversarial text for 5000 iterations with a batch size of 8, aligned with configurations for visual attacks. **This process imposes a computational overhead approximately 12 times greater than that associated with our visual attack, attributable to the greater computational demands inherent in the discrete optimization algorithm in the textual space.**

⁵https://support.perspectiveapi.com/s/docs-get-started?language=en_US

⁶<https://github.com/unitaryai/detoxify>

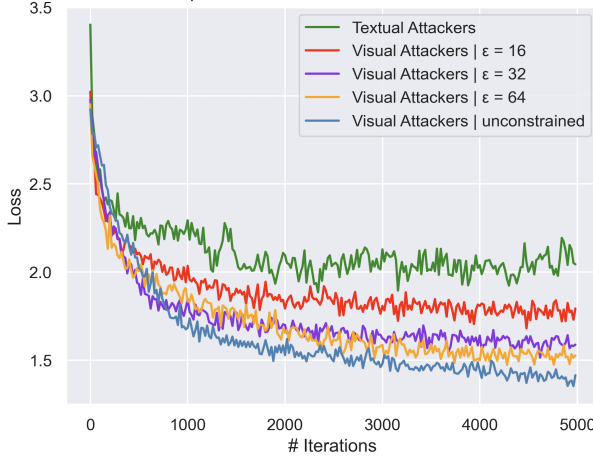


Figure 2: Comparison of optimization loss (on the adversarial objectives) among our visual attackers and a standard textual attacker [29]. For a fair comparison, we limit adversarial texts to 32 tokens, aligning with the length of an image in MiniGPT-4’s input embedding space [50].

constrained visual attack, which operates within a tight budget of $\epsilon = 16/255$, the adversarial text still lags in three out of the four harmful scenarios that we evaluate. To our surprise, the adversarial text even makes the violence/crime related instructions more likely to be refused by the model compared with the benign baseline without attack. When evaluated on the RealToxicityPrompts benchmark (Table 2), the adversarial text only matched the performance of the adversarial image subjected to the strictest constraint of $\epsilon = 16/255$, while trailing behind stronger visual attacks. **Collectively, these findings also underscore the more potent impact of our visual adversarial attacks.**

Comparison. We compare the effectiveness of our visual attacks and the textual attacks based on the capacity to minimize the loss values of the same adversarial objective (Eqn 2). The loss trajectories for these attacks are graphically presented in Figure 2. As shown, **the textual attacker fails to attain a level of success commensurate with the visual attack.** Despite the absence of stealthiness/naturalness constraints and the engagement of a computational effort 12 times greater, the discrete optimization within the textual space is still less effective than the continuous optimization (even the one subject to a tight ϵ constraints of $16/255$) within the visual space. This observation is consistent with our initial supposition, considering the visual input space is continuous and end-to-end differentiable with respect to the adversarial objective, while the textual space is discrete and non-differentiable.

We also engage in a quantitative assessment comparing the efficacy of textual attacks versus our visual attacks in terms of their success in compromising the model’s safety mechanisms. Our manual evaluation (Table 1) suggests that the unconstrained adversarial text consistently falls short of the performance of the unconstrained adversarial image. When contrasted with the

Table 3: The percentages of the generated outputs that exhibit certain toxic attributes given by Perspective API, tested on the RealToxicityPrompts *challenging* subset. DiffPure effectively reduces the probability of toxic degeneration across all toxicity attributes. The leftmost column is the percentage of the generated texts that exhibit *any* of the 6 attributes. For the full results across the other noise levels and the results of Detoxify classifier, see Table 4.

Input	Perspective API						Toxicity
	Any	Identity Attack	Profanity	Severe Toxicity	Sexually Explicit	Threat	
benign image without attack (baseline)	34.83% \pm 1.63%	2.69% \pm 0.24%	25.13% \pm 1.76%	1.54% \pm 0.17%	12.23% \pm 0.55%	2.02% \pm 0.13%	30.51% \pm 1.44%
adv. image ($\epsilon = 16/255$)	53.56% \pm 1.03%	8.37% \pm 0.42%	36.59% \pm 0.55%	6.59% \pm 0.52%	14.07% \pm 0.34%	4.74% \pm 0.31%	48.59% \pm 0.56%
+ DiffPure ($\sqrt{1-\alpha_t} = 0.5$)	37.50% \pm 0.83%	2.68% \pm 0.24%	26.43% \pm 0.92%	1.28% \pm 0.10%	13.05% \pm 0.08%	2.17% \pm 0.30%	31.31% \pm 0.87%
adv. image ($\epsilon = 32/255$)	59.36% \pm 1.36%	14.59% \pm 0.57%	39.53% \pm 1.21%	6.97% \pm 0.38%	14.87% \pm 0.92%	6.16% \pm 0.22%	53.75% \pm 1.01%
+ DiffPure ($\sqrt{1-\alpha_t} = 0.5$)	32.65% \pm 0.72%	1.68% \pm 0.41%	23.05% \pm 0.28%	1.06% \pm 0.11%	11.12% \pm 0.23%	1.76% \pm 0.25%	27.43% \pm 1.20%
adv. image ($\epsilon = 64/255$)	67.18% \pm 0.17%	15.91% \pm 0.18%	49.62% \pm 0.39%	12.15% \pm 0.50%	16.86% \pm 0.42%	6.60% \pm 0.48%	63.05% \pm 0.78%
+ DiffPure ($\sqrt{1-\alpha_t} = 0.5$)	37.12% \pm 0.97%	2.49% \pm 0.58%	26.37% \pm 0.76%	1.65% \pm 0.26%	12.12% \pm 0.31%	2.26% \pm 0.14%	31.82% \pm 0.69%
adv. image (unconstrained)	66.04% \pm 1.01%	17.41% \pm 1.23%	43.25% \pm 1.57%	7.96% \pm 0.43%	14.60% \pm 0.30%	7.04% \pm 0.96%	61.70% \pm 1.12%
+ DiffPure ($\sqrt{1-\alpha_t} = 0.5$)	32.76% \pm 0.41%	2.16% \pm 0.04%	22.41% \pm 0.53%	1.28% \pm 0.42%	11.58% \pm 0.65%	1.96% \pm 0.37%	27.99% \pm 0.45%

6 Analyzing Defenses against Our Attacks

In general, defending against visual adversarial examples is known to be fundamentally difficult [4; 8; 41] and continues to be an open problem. Despite advancements in adversarial training [28; 13] and robustness certification [12; 9; 46; 26] aimed at counteracting visual adversarial examples, they are not directly applicable to our setup. The gaps arise as these classical defenses are predominantly designed for classification tasks, heavily relying on the concept of discrete classes. This reliance becomes a major barrier when applying these defenses to LLMs, which have open-ended outputs, contrasting the narrowly defined settings of image classification.

Given this predicament, we steer our focus away from conventional adversarial training and robustness certification techniques, turning instead toward input preprocessing based defenses. In particular, we suggest the application of the recently developed DiffPure [30] to counter our visual adversarial examples. DiffPure mitigates adversarial input

by introducing noise to the image and then utilizes a diffusion model [22] to project the diffused image back to its learned data manifold. This technique operates under the presumption that the introduced noise will diminish the adversarial patterns and the pre-trained diffusion model can restore the clean image. Given its model and task independence, DiffPure can function as a plug-and-play module and be seamlessly integrated into our setup.

Specifically, we employ Stable Diffusion v1.5 [36], as it is trained on a diverse set of images. Our input to the diffusion model is the diffused image corresponding to the time index t : $x_t = \sqrt{\alpha_t}x_0 + \sqrt{1 - \alpha_t}\eta$, where $\eta \sim \mathcal{N}(0, I)$ represents the random noise. We select $\sqrt{1 - \alpha_t} \in \{0.25, 0.5, 0.75\}$ and follow the same evaluation method as Section 4.2. We observe that all three noise levels effectively purify our visual adversarial examples, with the results from Perspective API and Detoxify aligning well. We present the results for $\sqrt{1 - \alpha_t} = 0.5$ as evaluated by Perspective API in Table 3, deferring the complete results to Table 4. It is clear that DiffPure substantially lowers the likelihood of generating toxic content across all attributes, aligning with the toxicity level of the benign baseline without adversarial attacks.

Still, we note that DiffPure cannot entirely neutralize the inherent risks presented by our threat model in Sec 3.2. The effectiveness of the defense might falter when faced with more delicate adaptive attacks [18]. Additionally, while DiffPure can offer some level of protection to online models from attacks by malicious users, it provides no safeguards for offline models that may be deployed independently by attackers. These adversaries could primarily seek to exploit adversarial attacks to jailbreak the safety mechanisms of offline models and misuse them for malicious intentions. This situation also underscores the potential hazards associated with open-sourcing powerful LLMs.

7 Conclusion

In this work, we explore the expanded security risks associated with introducing vision into Large Language Models (LLMs). Our examinations reveal an increased vulnerability to adversarial attacks through the additional visual inputs. Moreover, the implications of the attacks extend beyond failure on a particular task. Through comprehensive evaluation, we demonstrate the practicality of using visual adversarial examples to undermine the safety mechanisms of LLMs, thereby facilitating the generation of harmful content. Particularly, we discover that a relatively simple approach can produce universal visual adversarial examples. These have the power to generally compromise the model’s safety mechanisms and steer the model to heed a wide range of harmful instructions. Committed to responsible disclosure, we suggest the utilization of DiffPure to counteract our adversarial attacks. However, we underscore that the inherent risks posed by our threat model may not be entirely resolved and necessitate continued efforts in the future. We advocate that, as we progress in the development of Visual Language Models (VLMs), we must concurrently evolve our understanding and strategies to mitigate the unique safety and security challenges they introduce. In doing so, we ensure that the evolution of these powerful tools is accompanied by robust safety measures, offering greater safety and ethical responsibility in their deployment.

References

- [1] J.-B. Alayrac, J. Donahue, P. Luc, A. Miech, I. Barr, Y. Hasson, K. Lenc, A. Mensch, K. Millican, M. Reynolds, et al. Flamingo: a visual language model for few-shot learning. *Advances in Neural Information Processing Systems*, 35:23716–23736, 2022. 1, 3
- [2] M. Alzantot, Y. Sharma, A. Elgohary, B.-J. Ho, M. Srivastava, and K.-W. Chang. Generating natural language adversarial examples. *arXiv preprint arXiv:1804.07998*, 2018. 2, 4
- [3] S. Antol, A. Agrawal, J. Lu, M. Mitchell, D. Batra, C. L. Zitnick, and D. Parikh. Vqa: Visual question answering. In *Proceedings of the IEEE international conference on computer vision*, pages 2425–2433, 2015. 1
- [4] A. Athalye, N. Carlini, and D. Wagner. Obfuscated gradients give a false sense of security: Circumventing defenses to adversarial examples. In *International conference on machine learning*, pages 274–283. PMLR, 2018. 2, 4, 8
- [5] Y. Bai, A. Jones, K. Ndousse, A. Askell, A. Chen, N. DasSarma, D. Drain, S. Fort, D. Ganguli, T. Henighan, N. Joseph, S. Kadavath, J. Kernion, T. Conerly, S. El-Showk, N. Elhage, Z. Hatfield-Dodds, D. Hernandez, T. Hume, S. Johnston, S. Kravec, L. Lovitt, N. Nanda, C. Olsson, D. Amodei, T. Brown, J. Clark, S. McCandlish, C. Olah, B. Mann, and J. Kaplan. Training a helpful and harmless assistant with reinforcement learning from human feedback, 2022. 4
- [6] R. Bommasani, D. A. Hudson, E. Adeli, R. Altman, S. Arora, S. von Arx, M. S. Bernstein, J. Bohg, A. Bosselut, E. Brunskill, et al. On the opportunities and risks of foundation models. *arXiv preprint arXiv:2108.07258*, 2021. 2

- [7] T. Brown, B. Mann, N. Ryder, M. Subbiah, J. D. Kaplan, P. Dhariwal, A. Neelakantan, P. Shyam, G. Sastry, A. Askell, et al. Language models are few-shot learners. *Advances in neural information processing systems*, 33:1877–1901, 2020. [1](#)
- [8] N. Carlini and D. Wagner. Adversarial examples are not easily detected: Bypassing ten detection methods. In *Proceedings of the 10th ACM workshop on artificial intelligence and security*, pages 3–14, 2017. [2, 4, 8](#)
- [9] N. Carlini, F. Tramer, J. Z. Kolter, et al. (certified!!) adversarial robustness for free! *arXiv preprint arXiv:2206.10550*, 2022. [8](#)
- [10] W.-L. Chiang, Z. Li, Z. Lin, Y. Sheng, Z. Wu, H. Zhang, L. Zheng, S. Zhuang, Y. Zhuang, J. E. Gonzalez, I. Stoica, and E. P. Xing. Vicuna: An open-source chatbot impressing gpt-4 with 90%* chatgpt quality, March 2023. URL <https://lmsys.org/blog/2023-03-30-vicuna/>. [2, 4](#)
- [11] J. Cho, J. Lei, H. Tan, and M. Bansal. Unifying vision-and-language tasks via text generation. In *International Conference on Machine Learning*, pages 1931–1942. PMLR, 2021. [1, 3](#)
- [12] J. Cohen, E. Rosenfeld, and Z. Kolter. Certified adversarial robustness via randomized smoothing. In *international conference on machine learning*, pages 1310–1320. PMLR, 2019. [8](#)
- [13] F. Croce, M. Andriushchenko, V. Schwag, E. Debenedetti, N. Flammarion, M. Chiang, P. Mittal, and M. Hein. Robustbench: a standardized adversarial robustness benchmark. *arXiv preprint arXiv:2010.09670*, 2020. [8](#)
- [14] W. Dai, J. Li, D. Li, A. M. H. Tiong, J. Zhao, W. Wang, B. Li, P. Fung, and S. Hoi. Instructblip: Towards general-purpose vision-language models with instruction tuning. *arXiv preprint arXiv:2305.06500*, 2023. [3](#)
- [15] D. Driess, F. Xia, M. S. Sajjadi, C. Lynch, A. Chowdhery, B. Ichter, A. Wahid, J. Tompson, Q. Vuong, T. Yu, et al. Palm-e: An embodied multimodal language model. *arXiv preprint arXiv:2303.03378*, 2023. [1](#)
- [16] J. Ebrahimi, A. Rao, D. Lowd, and D. Dou. Hotflip: White-box adversarial examples for text classification. *arXiv preprint arXiv:1712.06751*, 2017. [7](#)
- [17] Y. Fang, W. Wang, B. Xie, Q. Sun, L. Wu, X. Wang, T. Huang, X. Wang, and Y. Cao. Eva: Exploring the limits of masked visual representation learning at scale. In *Proceedings of the IEEE/CVF Conference on Computer Vision and Pattern Recognition*, pages 19358–19369, 2023. [2, 4](#)
- [18] Y. Gao, I. Shumailov, K. Fawaz, and N. Papernot. On the limitations of stochastic pre-processing defenses. *arXiv preprint arXiv:2206.09491*, 2022. [9](#)
- [19] S. Gehman, S. Gururangan, M. Sap, Y. Choi, and N. A. Smith. Realtocixityprompts: Evaluating neural toxic degeneration in language models. *arXiv preprint arXiv:2009.11462*, 2020. [2, 7](#)
- [20] I. J. Goodfellow, J. Shlens, and C. Szegedy. Explaining and harnessing adversarial examples. *arXiv preprint arXiv:1412.6572*, 2014. [2, 4](#)
- [21] J. Ho and T. Salimans. Classifier-free diffusion guidance. *arXiv preprint arXiv:2207.12598*, 2022. [12](#)
- [22] J. Ho, A. Jain, and P. Abbeel. Denoising diffusion probabilistic models. *Advances in Neural Information Processing Systems*, 33:6840–6851, 2020. [9](#)
- [23] A. Holtzman, J. Buys, L. Du, M. Forbes, and Y. Choi. The curious case of neural text degeneration. *arXiv preprint arXiv:1904.09751*, 2019. [6](#)
- [24] E. Jones, A. Dragan, A. Raghunathan, and J. Steinhardt. Automatically auditing large language models via discrete optimization. *arXiv preprint arXiv:2303.04381*, 2023. [2, 4](#)
- [25] J. Li, D. Li, S. Savarese, and S. Hoi. Blip-2: Bootstrapping language-image pre-training with frozen image encoders and large language models. *arXiv preprint arXiv:2301.12597*, 2023. [1, 3, 4](#)
- [26] L. Li, T. Xie, and B. Li. Sok: Certified robustness for deep neural networks. In *44th IEEE Symposium on Security and Privacy, SP 2023, San Francisco, CA, USA, 22-26 May 2023*. IEEE, 2023. [8](#)
- [27] Y. Liu, G. Deng, Z. Xu, Y. Li, Y. Zheng, Y. Zhang, L. Zhao, T. Zhang, and Y. Liu. Jailbreaking chatgpt via prompt engineering: An empirical study. *arXiv preprint arXiv:2305.13860*, 2023. [2](#)
- [28] A. Madry, A. Makelov, L. Schmidt, D. Tsipras, and A. Vladu. Towards deep learning models resistant to adversarial attacks. *arXiv preprint arXiv:1706.06083*, 2017. [2, 4, 5, 8](#)
- [29] N. Mehrabi, A. Beirami, F. Morstatter, and A. Galstyan. Robust conversational agents against imperceptible toxicity triggers. In *Proceedings of the 2022 Conference of the North American Chapter of the Association for Computational Linguistics: Human Language Technologies*, pages 2831–2847, Seattle, United States, July 2022. Association for Computational Linguistics. doi:[10.18653/v1/2022.naacl-main.204](https://doi.org/10.18653/v1/2022.naacl-main.204). URL <https://aclanthology.org/2022.naacl-main.204>. [7, 8](#)

- [30] W. Nie, B. Guo, Y. Huang, C. Xiao, A. Vahdat, and A. Anandkumar. Diffusion models for adversarial purification. *arXiv preprint arXiv:2205.07460*, 2022. 8
- [31] OpenAI. Introducing ChatGPT. <https://openai.com/blog/chatgpt>, 2022. 1, 4
- [32] OpenAI. Gpt-4 technical report, 2023. 1, 2, 3, 4
- [33] OpenAI. Our approach to ai safety. <https://openai.com/blog/our-approach-to-ai-safety>, 2023. [Online; accessed 24-May-2023]. 2
- [34] OpenAI. Forecasting potential misuses of language models for disinformation campaigns and how to reduce risk. <https://openai.com/research/forecasting-misuse>, 2023. [Online; accessed 4-Apr-2023]. 2
- [35] L. Ouyang, J. Wu, X. Jiang, D. Almeida, C. Wainwright, P. Mishkin, C. Zhang, S. Agarwal, K. Slama, A. Ray, et al. Training language models to follow instructions with human feedback. *Advances in Neural Information Processing Systems*, 35:27730–27744, 2022. 4
- [36] R. Rombach, A. Blattmann, D. Lorenz, P. Esser, and B. Ommer. High-resolution image synthesis with latent diffusion models. In *Proceedings of the IEEE/CVF Conference on Computer Vision and Pattern Recognition*, pages 10684–10695, 2022. 9
- [37] T. Schick, S. Udupa, and H. Schütze. Self-diagnosis and self-debiasing: A proposal for reducing corpus-based bias in nlp. *Transactions of the Association for Computational Linguistics*, 9:1408–1424, 2021. 7
- [38] J. Song, C. Meng, and S. Ermon. Denoising diffusion implicit models. *arXiv preprint arXiv:2010.02502*, 2020. 12
- [39] C. Szegedy, W. Zaremba, I. Sutskever, J. Bruna, D. Erhan, I. Goodfellow, and R. Fergus. Intriguing properties of neural networks. *arXiv preprint arXiv:1312.6199*, 2013. 4
- [40] H. Touvron, T. Lavril, G. Izacard, X. Martinet, M.-A. Lachaux, T. Lacroix, B. Rozière, N. Goyal, E. Hambro, F. Azhar, et al. Llama: Open and efficient foundation language models. *arXiv preprint arXiv:2302.13971*, 2023. 4
- [41] F. Tramer. Detecting adversarial examples is (nearly) as hard as classifying them. In *International Conference on Machine Learning*, pages 21692–21702. PMLR, 2022. 2, 4, 8
- [42] E. Wallace, S. Feng, N. Kandpal, M. Gardner, and S. Singh. Universal adversarial triggers for attacking and analyzing nlp. *arXiv preprint arXiv:1908.07125*, 2019. 2, 4, 7
- [43] B. Wang, H. Pei, B. Pan, Q. Chen, S. Wang, and B. Li. T3: Tree-autoencoder constrained adversarial text generation for targeted attack. *arXiv preprint arXiv:1912.10375*, 2019. 4
- [44] W. Wang, Z. Chen, X. Chen, J. Wu, X. Zhu, G. Zeng, P. Luo, T. Lu, J. Zhou, Y. Qiao, and J. Dai. Visionllm: Large language model is also an open-ended decoder for vision-centric tasks, 2023. 3
- [45] Y. Wang, Y. Kordi, S. Mishra, A. Liu, N. A. Smith, D. Khashabi, and H. Hajishirzi. Self-instruct: Aligning language models with self-generated instructions, 2023. 4
- [46] C. Xiang, S. Mahloujifar, and P. Mittal. {PatchCleanser}: Certifiably robust defense against adversarial patches for any image classifier. In *31st USENIX Security Symposium (USENIX Security 22)*, pages 2065–2082, 2022. 8
- [47] J. Xu, D. Ju, M. Li, Y.-L. Boureau, J. Weston, and E. Dinan. Recipes for safety in open-domain chatbots. *arXiv preprint arXiv:2010.07079*, 2020. 4
- [48] R. Zellers, Y. Bisk, A. Farhadi, and Y. Choi. From recognition to cognition: Visual commonsense reasoning. In *Proceedings of the IEEE/CVF conference on computer vision and pattern recognition*, pages 6720–6731, 2019. 1
- [49] Z. Zhao, D. Dua, and S. Singh. Generating natural adversarial examples. *arXiv preprint arXiv:1710.11342*, 2017. 2, 4
- [50] D. Zhu, J. Chen, X. Shen, X. Li, and M. Elhoseiny. Minigpt-4: Enhancing vision-language understanding with advanced large language models. *arXiv preprint arXiv:2304.10592*, 2023. 1, 2, 3, 4, 8

A Additional Experimental Details

A.1 MiniGPT-4 Chatbot Text Template

MiniGPT-4 builds off the v0 version of the Vicuna model. As Vicuna is a chatbot-style language model, MiniGPT-4 wraps the image embeddings and user inputs into the same chatbot format as Vicuna v0 model⁷ with the following text template :

<System Message> ### Human: <ImageHere> <Input> ### Assistant:

Specifically, *<System Message>* is a description of the conversation, which regulates the behavior of the Vicuna model. *<ImageHere>* is a placeholder and will be replaced by the image embedding vectors after the user uploads the image. The user text input is appended to the image embeddings. Given the wrapped prompt, Vicuna autoregressively generates its continuation as the reply of the Assistant.

System Messages. For MiniGPT-4, the default system message is “Give the following image: *ImageContent*. You will be able to see the image once I provide it to you. Please answer my questions.”.⁸ We choose this system message for both image-based adversarial attacks and text-based adversarial attacks.

Sentence Completion. To evaluate the performance on the RealToxicityPrompts dataset, we turn the model into a “language model” that completes the user input sentence. Specifically, we wrap each input using the following text template with the explicit instruction to prompt MiniGPT-4 to perform sentence continuation:

<System Message> ### Human: <ImageHere> Please extend the following sentence: <input> ### Assistant:

A.2 Full Results and Implementation Details for DiffPure (Section 6)

As Stable Diffusion is a text-conditioned diffusion model, we choose an uninformative text prompt “An image.” in our experiments. We use the default DDIM sampler [38] but we disable the classifier-free guidance [21] as the text prompt contains no useful information for guidance.

⁷https://github.com/lm-sys/FastChat/blob/main/docs/vicuna_weights_version.md

⁸<https://github.com/Vision-CAIR/MiniGPT-4/blob/main/minigpt4/conversation/conversation.py>

Input	Any	Identity Attack	Perspective API Profanity	Severe Toxicity	Sexually Explicit	Threat	Toxicity
benign image without attack (baseline)	34.83% \pm 1.63%	2.69% \pm 0.24%	25.13% \pm 1.76%	1.54% \pm 0.17%	12.23% \pm 0.55%	2.02% \pm 0.13%	30.51% \pm 1.44%
adv. image ($\epsilon = 16/255$)	53.56% \pm 1.03%	8.37% \pm 0.42%	36.59% \pm 0.55%	6.59% \pm 0.52%	14.07% \pm 0.34%	4.74% \pm 0.31%	48.59% \pm 0.56%
+ DiffPure ($\sqrt{1-\alpha_t} = 0.75$)	48.08% \pm 0.77%	3.54% \pm 0.17%	34.47% \pm 0.98%	2.20% \pm 0.72%	14.81% \pm 0.57%	3.12% \pm 0.52%	41.49% \pm 0.91%
+ DiffPure ($\sqrt{1-\alpha_t} = 0.5$)	37.50% \pm 0.83%	2.68% \pm 0.24%	26.43% \pm 0.92%	1.28% \pm 0.10%	13.05% \pm 0.08%	2.17% \pm 0.30%	31.31% \pm 0.87%
+ DiffPure ($\sqrt{1-\alpha_t} = 0.25$)	49.79% \pm 0.99%	3.98% \pm 0.22%	36.78% \pm 0.91%	2.42% \pm 0.07%	14.88% \pm 0.37%	2.81% \pm 0.28%	43.58% \pm 1.19%
adv. image ($\epsilon = 32/255$)	59.36% \pm 1.36%	14.59% \pm 0.57%	39.53% \pm 1.21%	6.97% \pm 0.38%	14.87% \pm 0.92%	6.16% \pm 0.22%	53.75% \pm 1.01%
+ DiffPure ($\sqrt{1-\alpha_t} = 0.75$)	36.14% \pm 1.57%	2.43% \pm 0.18%	24.92% \pm 1.86%	1.03% \pm 0.35%	12.45% \pm 0.25%	1.93% \pm 0.36%	30.34% \pm 1.16%
+ DiffPure ($\sqrt{1-\alpha_t} = 0.5$)	32.65% \pm 0.72%	1.68% \pm 0.41%	23.05% \pm 0.28%	1.06% \pm 0.11%	11.12% \pm 0.23%	1.76% \pm 0.25%	27.43% \pm 1.20%
+ DiffPure ($\sqrt{1-\alpha_t} = 0.25$)	48.80% \pm 1.39%	3.60% \pm 0.55%	35.19% \pm 1.60%	2.23% \pm 0.40%	15.53% \pm 0.35%	2.57% \pm 0.16%	42.75% \pm 1.49%
adv. image ($\epsilon = 64/255$)	67.18% \pm 0.17%	15.91% \pm 0.18%	49.62% \pm 0.39%	12.15% \pm 0.50%	16.86% \pm 0.42%	6.60% \pm 0.48%	63.05% \pm 0.78%
+ DiffPure ($\sqrt{1-\alpha_t} = 0.75$)	39.30% \pm 2.54%	2.75% \pm 0.29%	27.60% \pm 1.57%	1.63% \pm 0.22%	12.77% \pm 1.05%	2.41% \pm 0.31%	33.74% \pm 1.68%
+ DiffPure ($\sqrt{1-\alpha_t} = 0.5$)	37.12% \pm 0.97%	2.49% \pm 0.58%	26.37% \pm 0.76%	1.65% \pm 0.26%	12.12% \pm 0.31%	2.26% \pm 0.14%	31.82% \pm 0.69%
+ DiffPure ($\sqrt{1-\alpha_t} = 0.25$)	29.88% \pm 0.41%	1.63% \pm 0.25%	20.52% \pm 0.80%	0.87% \pm 0.28%	10.68% \pm 0.21%	1.55% \pm 0.24%	25.30% \pm 0.66%
adv. image (unconstrained)	66.04% \pm 1.01%	17.41% \pm 1.23%	43.25% \pm 1.57%	7.96% \pm 0.43%	14.60% \pm 0.30%	7.04% \pm 0.96%	61.70% \pm 1.12%
+ DiffPure ($\sqrt{1-\alpha_t} = 0.75$)	31.01% \pm 0.24%	2.11% \pm 0.15%	22.04% \pm 0.57%	0.71% \pm 0.21%	10.82% \pm 0.24%	1.34% \pm 0.15%	26.05% \pm 0.45%
+ DiffPure ($\sqrt{1-\alpha_t} = 0.5$)	32.76% \pm 0.41%	2.16% \pm 0.04%	22.41% \pm 0.53%	1.28% \pm 0.42%	11.58% \pm 0.65%	1.96% \pm 0.37%	27.99% \pm 0.45%
+ DiffPure ($\sqrt{1-\alpha_t} = 0.25$)	33.84% \pm 1.12%	2.34% \pm 0.39%	24.05% \pm 0.21%	1.31% \pm 0.20%	12.41% \pm 0.81%	2.03% \pm 0.17%	28.73% \pm 0.89%

Input	Any	Identity Attack	Detoxify Obscene	Severe Toxicity	Insult	Threat	Toxicity
benign image without attack (baseline)	29.08% \pm 0.95%	1.49% \pm 0.04%	22.41% \pm 1.54%	0.62% \pm 0.04%	10.99% \pm 0.89%	0.87% \pm 0.10%	28.86% \pm 0.91%
adv. image ($\epsilon = 16/255$)	46.39% \pm 1.13%	5.02% \pm 0.43%	33.66% \pm 0.59%	2.29% \pm 0.39%	23.64% \pm 0.35%	2.18% \pm 0.07%	46.13% \pm 0.97%
+ DiffPure ($\sqrt{1-\alpha_t} = 0.75$)	38.90% \pm 1.06%	1.73% \pm 0.14%	30.51% \pm 0.85%	0.53% \pm 0.08%	15.45% \pm 0.74%	1.31% \pm 0.32%	38.29% \pm 1.09%
+ DiffPure ($\sqrt{1-\alpha_t} = 0.5$)	29.63% \pm 0.72%	1.17% \pm 0.07%	23.56% \pm 0.34%	0.47% \pm 0.08%	10.51% \pm 0.44%	0.75% \pm 0.07%	28.91% \pm 0.66%
+ DiffPure ($\sqrt{1-\alpha_t} = 0.25$)	40.54% \pm 0.59%	1.62% \pm 0.38%	32.68% \pm 0.89%	0.89% \pm 0.04%	15.41% \pm 1.11%	1.14% \pm 0.08%	39.87% \pm 0.55%
adv. image ($\epsilon = 32/255$)	51.32% \pm 1.47%	9.71% \pm 0.38%	38.16% \pm 1.55%	2.73% \pm 0.55%	26.14% \pm 0.62%	2.62% \pm 0.26%	50.88% \pm 1.43%
+ DiffPure ($\sqrt{1-\alpha_t} = 0.75$)	28.41% \pm 1.53%	1.06% \pm 0.28%	21.77% \pm 1.56%	0.28% \pm 0.22%	9.88% \pm 1.01%	0.89% \pm 0.21%	28.05% \pm 1.50%
+ DiffPure ($\sqrt{1-\alpha_t} = 0.5$)	26.29% \pm 0.25%	0.87% \pm 0.17%	20.28% \pm 0.27%	0.34% \pm 0.07%	9.05% \pm 0.43%	0.75% \pm 0.07%	25.92% \pm 0.41%
+ DiffPure ($\sqrt{1-\alpha_t} = 0.25$)	39.32% \pm 1.19%	1.81% \pm 0.04%	30.57% \pm 1.40%	0.59% \pm 0.14%	14.61% \pm 0.70%	1.03% \pm 0.28%	38.76% \pm 1.05%
adv. image ($\epsilon = 64/255$)	61.44% \pm 0.84%	11.70% \pm 0.30%	49.26% \pm 0.07%	5.35% \pm 0.47%	36.44% \pm 0.70%	3.15% \pm 0.38%	61.13% \pm 0.73%
+ DiffPure ($\sqrt{1-\alpha_t} = 0.75$)	31.89% \pm 1.73%	1.52% \pm 0.18%	25.04% \pm 1.68%	0.59% \pm 0.14%	12.07% \pm 0.79%	1.04% \pm 0.24%	31.36% \pm 1.72%
+ DiffPure ($\sqrt{1-\alpha_t} = 0.5$)	30.92% \pm 0.63%	1.06% \pm 0.16%	23.99% \pm 0.15%	0.56% \pm 0.08%	10.84% \pm 0.44%	1.03% \pm 0.14%	30.28% \pm 0.57%
+ DiffPure ($\sqrt{1-\alpha_t} = 0.25$)	23.03% \pm 0.49%	0.84% \pm 0.18%	17.71% \pm 0.18%	0.37% \pm 0.04%	7.73% \pm 0.20%	0.59% \pm 0.07%	22.69% \pm 0.38%
adv. image (unconstrained)	60.97% \pm 1.54%	10.15% \pm 0.56%	42.39% \pm 1.05%	2.59% \pm 0.12%	32.66% \pm 1.17%	2.75% \pm 0.35%	60.70% \pm 1.60%
+ DiffPure ($\sqrt{1-\alpha_t} = 0.75$)	24.91% \pm 0.77%	1.25% \pm 0.10%	19.13% \pm 1.06%	0.31% \pm 0.04%	9.03% \pm 0.73%	0.60% \pm 0.18%	24.54% \pm 0.80%
+ DiffPure ($\sqrt{1-\alpha_t} = 0.5$)	26.22% \pm 0.15%	1.14% \pm 0.14%	19.88% \pm 0.35%	0.48% \pm 0.08%	9.90% \pm 0.74%	1.05% \pm 0.31%	25.82% \pm 0.03%
+ DiffPure ($\sqrt{1-\alpha_t} = 0.25$)	26.73% \pm 1.28%	1.17% \pm 0.15%	20.66% \pm 0.34%	0.63% \pm 0.15%	9.56% \pm 0.25%	1.11% \pm 0.07%	26.51% \pm 1.32%

Table 4: The percentages of the generated outputs that exhibit certain toxic attributes given by Perspective API and Detoxify Classifier, tested on the RealToxicityPrompts *challenging* subset. We see that DiffPure methods across noise level $\sqrt{1-\alpha_t} \in \{0.25, 0.5, 0.75\}$ significantly reduce the probabilities of generating toxic outputs that exhibit various attributes. The leftmost column is the percentage of the generated texts that exhibit *any* of the 6 attributes.